Electron Irradiation of Copper Near 10°K

J. W. CORBETT, J. M. DENNEY,* M. D. FISKE, AND R. M. WALKER
General Electric Research Laboratory, Schenectady, New York

(Received July 16, 1957)

The resistivity change induced by electron irradiation of zone-refined copper maintained at ~10°K has been measured over the range of bombarding electron energies from 0.70 to 1.37 Mev. The cross section for damage production is shown to be insensitive to the choice of the shape of the displacement probability function for this energy range. An "average" threshold energy for displacement of 22±3 ev is deduced, from which the resistivity of Frenkel pairs, $\rho_f = 1.45 \pm 0.5$ μohm cm/atomic % is obtained. Isochronal and isothermal annealing studies of irradiations performed at 1.37 Mev are described. The maximum annealing rate, as obtained from an isochronal anneal, occurs at ~40°K; ~90% of the irradiation-induced resistivity annealing out in the range 20°K–65°K. The isothermal annealing curves are not amenable to analysis in terms of a single simple rate process, but seem to require a multiplicity of processes.

INTRODUCTION

A GREAT deal of excellent work has gone into experiments designed to elucidate the nature of the radiation-damage process in metals, but a generally accepted model has not yet been obtained.[1] The issue has been partially obscured by the fact that the early experiments were performed at specimen temperatures where the damage products could undergo change during bombardment. For this reason, the more recent experiments have been carried out at low temperatures; namely deuteron irradiations near 10°K,[2] and neutron irradiations below 22°K.[3]

Deuteron and neutron irradiations are inherently difficult to treat theoretically, since heavy particles are capable of imparting a large amount of energy to the lattice in a single collision, thereby possibly producing a multiplicity of defects. Irradiation, in which the energy given to a lattice atom is sufficient to displace only it alone, can be performed using electrons of about 1-Mev energy. The properties of damage products produced with electron irradiation should be more readily comparable with theory than those produced with heavy-particle irradiations. Such electron irradiations have been performed on copper at ~80°K by Eggen and Laubenstein[4] and by Meechan and Brinkman.[5]

The present paper describes the measurements of the electrical resistivity change in copper induced by electron irradiation performed at ~10°K.[6] The resistivity change is investigated as a function of the electron flux, the energy of the bombarding electrons, and the specimen temperature. Recovery through annealing was studied using both isothermal and isochronal pulse anneals.

EXPERIMENTAL APPARATUS

A cryostat was designed to permit electron irradiation of the specimens below 10°K, and subsequent *in situ* annealing at any temperature between 4°K and 400°K. The design permitted the measurement of two defect-sensitive properties: electrical resistivity, employed in the experiments reported here; and lattice parameter, to be employed in future experiments. Figure 1 is a schematic drawing of the cryostat. The specimen is located in a "pillbox" in the horizontal arm at the left, allowing passage of the vertical beam of the electron accelerator. A reservoir in the cryostat proper contains liquid helium from which helium can be pumped through the pillbox following the technique employed by Swenson.[7] For temperatures higher than 4.2°K, control was provided by adjustment of the helium pumping rate and simultaneous adjustment of

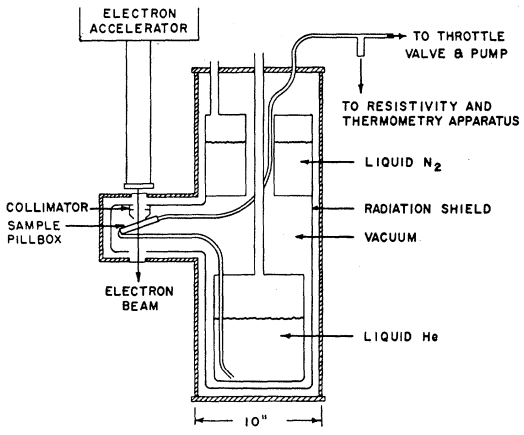

FIG. 1. Schematic drawing of electron-damage cryostat.

* Present address: Aeronutronic Systems, Inc., Glendale, California.

[1] For recent reviews of the field, see F. Seitz and J. S. Koehler, in *Solid State Physics* (Academic Press, Inc., New York, 1955), Vol. 2, p. 305; H. Brooks, in *Annual Reviews of Nuclear Science* (Annual Reviews, Inc., Stanford, 1956), Vol. 6, p. 215.

[2] Cooper, Koehler, and Marx, Phys. Rev. **97**, 599 (1955); R. O. Simmons and R. W. Balluffi, Bull. Am. Phys. Soc. Ser. II, **2**, 151 (1957).

[3] T. H. Blewitt *et al.*, Bull. Am. Phys. Soc. Ser. II, **1**, 130 (1956); **2**, 151 (1957).

[4] D. T. Eggen and M. J. Laubenstein, Phys. Rev. **91**, 238 (1953).

[5] C. J. Meechan and J. A. Brinkman, Phys. Rev. **103**, 1193 (1956).

[6] A preliminary account of this work was reported by the authors in Phys. Rev. **104**, 851 (1956).

[7] C. A. Swenson, Rev. Sci. Instr. **25**, 608 (1954).

the power supplied to a heater cemented to the pillbox exterior. This temperature control system keeps the sample cold during irradiation and permits subsequent pulse-annealing studies on the accumulated damage products. The specimen temperature can be raised from 4°K to ~60°K in one minute, the last five degrees taking ~20 seconds. Cooling the specimen from 60°K to ~4°K takes ~45 sec, the first five degrees taking less than two seconds.

A view of the pillbox as seen from above is shown in Fig. 2. The specimen is completely immersed in the refrigerant bath, in order to keep the specimen temperature below 10°K during irradiation for beam current densities as high as 10 μa cm^{-2}. The pillbox is made of a pair of beryllium-copper plates machined to provide internal space for the specimen, and is sealed with an annealed aluminum gasket. A beryllium window 0.008 in. thick and $\frac{1}{2}$ in. in diameter was silver-soldered into each plate. Beryllium was chosen to minimize energy loss in the electron beam passing through the assembly.

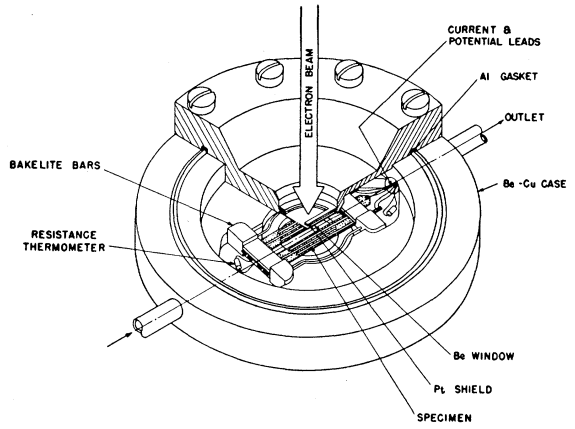

FIG. 2. Detail drawing of sample pillbox as seen from above.

With this design, only about 10% of the beam power is absorbed at helium temperatures, with consequent reduction in the requirement for liquid helium. Two specimens, one active and one control, were mounted in the pillbox. A 0.020-in. thick platinum shield with a half-moon shaped opening protected the control specimen from irradiation, and allowed the beam to pass through the active specimen.

The specimen was made in the form of a thin foil, in order to achieve homogeneous defect production throughout its thickness. American Smelting and Refining Company copper of 99.999% stated purity was zone-refined, rolled to 0.0032 cm thickness, and annealed for $\frac{1}{2}$ hour at 450°C, producing a material with 1.5×10^{-9} ohm cm resistivity at 4.2°K. The foil thickness represents about 4% of the electron range at 1.4 Mev, yet is sufficiently large that surface scattering of the conduction electrons does not overwhelm the defect scattering contribution to the electrical resistance

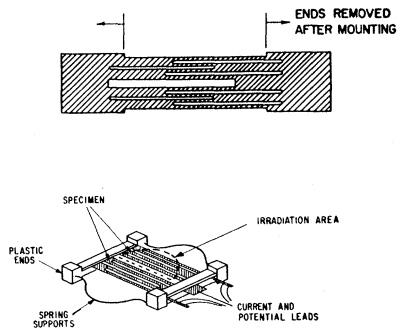

FIG. 3. Detail drawing of specimen. The upper drawing shows the sample before the active and control specimens have been separated. The lower drawing shows the specimen mounted in its Bakelite and wire holder. In this drawing the sample ends have been clipped and the active and control specimens separated.

of the specimen at 4.2°K. The annealed foil was carefully cemented with beeswax to a copper plate for protection in handling, and was photoengraved by a commercial process[8] to produce the pattern shown in Fig. 3. This pattern is a 20-fold photoreduction of an accurately drawn master, leading to specimens which have desired dimensions within $\pm$0.002 cm. The pattern of lengthwise slits maximizes the resistance length in the irradiated area. Both specimens, the one that is irradiated and the control, are formed in one piece.

The prepared specimen pair was mounted at the ends on Bakelite bars, and held in slight tension by spring steel wires joining the bars. The specimen ends then were clipped, as shown in Fig. 3, separating the two specimens, and the assembly was placed in the pillbox and two current and three potential leads were attached.

Thermometry was provided by calibrated carbon resistance thermometers placed in the fluid streams entering and leaving the pillbox; by an Au—Co *vs* Ag—Au thermocouple in the exit stream adjacent to the specimen; by a copper-constantan thermocouple mounted on the exterior of the pillbox; and finally by the temperature-dependent resistance of the copper specimen itself, which fitted a Grüneisen function within experimental accuracy. The internal consistency of the thermometers was such that the specimen temperature could be determined to within 0.5°K over the range 4°K to 400°K, and could be reset to the same temperature to within 0.1°K.

The voltage drop, at constant current, across one of the resistor-thermometers in the gas stream was monitored on a chart potentiometer for continuous displaying and recording of the pillbox temperature. All of the electrical leads from the pillbox passed up the pumping line and out of the cryostat through a wax seal at room temperature.

The temperature of the specimen itself during bombardment could be estimated in a variety of ways,

[8] We are indebted to J. M. Lafferty of this Laboratory for discussions of this technique, and H. F. Hart of the Maqua Company for photoengraving our specimens.

none of very high accuracy but all agreeing on an upper limit below 13°K, with probable values below 10°K. For a run at 1.37 Mev, and a current density of 1 μa/cm^2 with a helium flow of 0.4 cubic ft/min (STP), the pillbox inlet resistor would indicate 4.2°K, the outlet resistor 12°K, and the Au—Co *vs* Ag—Au thermocouple 13°K. The very small temperature-dependent resistance of the specimen indicated peak temperatures between 4°K and 12°K, the uncertainty arising from lack of precision in the beam-on measurements of the resistance. Simple heat-transfer calculations indicate that the maximum power of 0.05 watt cm^{-2} absorbed from the beam by the specimen should not raise its temperature above 7°K. The higher temperatures indicated by the down-stream thermometers may be attributed to general pillbox heating arising from inadequate electron-beam collimation and from beam absorption in the windows.

Specimen resistance was measured potentiometrically using a Rubicon 6-Dial Thermofree Potentiometer and current-emf switching arrangement to correct for thermal emf's. The current through the specimen during measurement was 0.3 ampere, and was regulated by a servomechanism to 1 part in 10^5. The precision of a typical series of resistance measurements was $\pm 6\times 10^{-8}$ ohm corresponding to a resistivity uncertainty of $\pm 1\times 10^{-12}$ ohm cm.

The source of high-energy electrons was a commercial-model General Electric resonant transformer. This accelerator, which normally produces a half sine wave of voltage, was equipped in this experiment with a gating circuit that selected a voltage pulse about 34° wide overlapping the peak value of voltage. The peak internal machine voltage was deduced from the resonant-circuit charging current, which was continually monitored during operation. This voltage should be linearly proportional to the charging current. To establish the linearity, the ratio of peak voltage to charging current was determined at high energies by the Be(γ,n) (1.655 Mev) reaction and at 100 kev by a spark-gap measurement. The ratios so determined were the same within 2%.

Accurate determination of the beam current and voltage is complicated by the effects of multiple scattering and energy straggling introduced by the various windows between the internal accelerator beam and the sample. The beam passes first through a 0.0027-in. stainless steel window on the accelerator snout, then through 5 cm of air, and enters the cryostat through another 0.0005-in. stainless steel window. Once inside the cryostat, the beam passes through a collimator which consists of an aluminum tube with two platinum aperture disks, and thence to the sample pillbox. The collimator is necessary to reduce the spray of high-energy electrons striking the pillbox which would cause an inordinate amount of liquid helium loss.

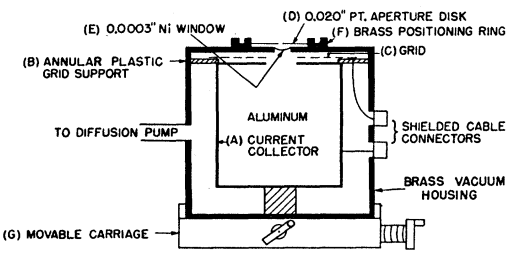

FIG. 4. Schematic drawing of Faraday cage assembly used to measure the distribution of current density in the electron beam incident upon the sample.

The primary calibration of current was not made in the actual cryostat arrangement but rather in a replica of the cryostat window and collimator geometry, before and after irradiation runs. This was done in order to use the greater absolute accuracy inherent in a Faraday-cage determination. An aluminum plate mounted below the pillbox was used with an integrating circuit to monitor the beam current during a run. Measurements of the current collected by this plate in the cryostat and in the replica were made to ensure the equivalent geometries of the two arrangements.

The simplest quantity to relate to an observed resistivity change is not the total beam current but rather the current density incident upon the sample. The Faraday cage shown schematically in Fig. 4 was used to measure the current density over the dimensions of the sample. The cage was designed so that virtually all the electrons that passed through a small test aperture were collected by the cup A. The test aperture consisted of a 0.020-in.-thick piece of platinum with a $\frac{1}{8}$-in. hole in the center. Platinum was chosen to minimize the number of electrons scattered into the hole from the sides. Preliminary measurements with several aperture sizes in conjunction with beam-distribution measurements showed that the geometrically measured area of the $\frac{1}{8}$-in. hole was a valid measure of the effective aperture for the electron beam. The grid was inserted to eliminate low-energy secondary electrons from the entrance foil, but voltages up to -2000 v showed only a small ($<2\%$) effect on the measured cage current.

The Faraday cage was mounted on a carriage that could be moved precisely in two mutually perpendicular directions, and the variation in current density was measured over the dimensions of the sample. There is a variation of about 10% in current density over the irradiated specimen width. At low beam energies the collection efficiency of the current collector is lowered due to increased multiple scattering in the entrance foil and a series of independent measurements was made with several collection-plate configurations to get reliable values for the current. Corrections for secondary emission were made by using the data of Miller and Porter.[9] All current measurements were made with and without a lead cover over the cage to eliminate the effects of x-rays and stray pickup. Al-

[9] B. L. Miller and W. C. Porter, J. Franklin Inst. **260**, 31 (1955).

though the above measurements are precise to ±2%, the uncertainty in the exact position (±$\frac{1}{16}$ in.) of the sample pillbox during irradiation introduces a ±10% uncertainty in the absolute current density.

In order to determine whether the collimator introduced a significant number of low-energy secondaries into the electron beam, measurements were made of the change in current density produced by various thicknesses of aluminum placed above the test aperture. The percentage decrease in current density for a given aluminum thickness was the same within 2%, both with and without the collimator, at all energies used in the experiment, showing that the collimator did not introduce an undesirable low-energy background.

An independent estimate of the product of voltage and current was obtained by measuring the heating effect of the beam. An aluminum disk thick enough to stop all the electrons was mounted in the Faraday cage directly under the entrance foil. The temperature rise in the disk was measured for 1-minute irradiations and the beam power was deduced from the known heat capacity of the disk. This heat capacity was directly determined by measuring the temperature rise in the disk resulting from a measured energy input to a small resistance heater glued to the disk. The heat capacity so determined agreed within 2% with the value calculated from the specific heat and the measured weight of the disk and resistor assembly.

In order to convert the directly measured resistance change of the foil to the desired change in bulk resistivity it is necessary to take into account both the fact that only part of the foil is irradiated and that part of the resistance change is due to a change in boundary scattering. Consider first the question of partial irradiation of the sample. Given a foil of length L and cross-sectional area A, let the length L_i be irradiated and the length $L_u=L-L_i$ remain unirradiated. If the resistivity of the irradiated portion is ρ_i' and that of the unirradiated is ρ_u', then the measured resistances R_b and R_a before and after irradiation, respectively, will be

$$R_b=\rho_u'L/A,$$
$$R_a=\rho_u'L_u/A+\rho_i'L_i/A. \quad (1)$$

The area A can be eliminated by using the expression for the room-temperature resistance R_{rm}:

$$R_{rm}=\rho_{rm}L/A. \quad (2)$$

Combining (1) and (2) and solving for the resistivity of the irradiated portion ρ_i' gives

$$\rho_i'=\rho_{rm}(LR_a-L_uR_b)/LR_{rm}. \quad (3)$$

Of the quantities on the right hand side of this equation, R_a, R_b, and R_{rm} are directly measured. The room temperature resistivity ρ_{rm} was calculated using the value 1.55 μohm cm at 0°C and a temperature coefficient of 3.93×10^{-3}/deg C for the resistivity of copper. The irradiated length L_i is known from the geometry of the sample and the beam collimator, and the unirradiated length L_u is known from the relationship $L_u=L-L_i$. The actual sample has a complicated shape and it is necessary to redefine L as an effective foil length. In principle L can be deduced from the geometry of the foil; but it was simpler to determine the ratio of effective length to geometric length by making resistance measurements on a large replica of accurately known dimensions and resistivity.

If there were no surface contribution to the resistance of the foil, or if the surface contribution were independent of irradiation, the increase in bulk resistivity produced by irradiation would be simply

$$\Delta\rho_i'=\rho_i'-\rho_u'=\rho_{rm}L(R_a-R_b)/L_iR_{rm}. \quad (4)$$

Unfortunately, however, the surface contribution to ρ_i' and ρ_u' is large (~30%) and changes with irradiation. For this reason ρ_i' and ρ_u' need to be corrected separately before they are subtracted. The corrected values of bulk resistivity will be represented by ρ_i and ρ_u for the irradiated and unirradiated materials respectively, and their difference by $\Delta\rho_i$,

$$\Delta\rho_i=\rho_i-\rho_u. \quad (5)$$

The corrections were taken directly from Sondheimer's theory[10] assuming diffuse surface scattering. They amounted to a decrease of approximately 30% in converting ρ_i' and ρ_u' to ρ_i and ρ_u, and to an increase of about 2% in $\Delta\rho_i$ relative to the more approximate $\Delta\rho_i'$. This correction, which is only approximate, would have been much greater had the foil been thinner.

EXPERIMENTAL RESULTS

The bulk resistivity changes $\Delta\rho_i$ produced by electron irradiation, during different runs at an average beam energy of 1.37 Mev, are given in the next to last column of Table I. In each of these runs the graph of $\Delta\rho_i$ *vs* electron dose was accurately linear. The values of $\Delta\rho_i$ for the standard dose of one electron/cm² will be denoted by $\Delta\rho_e$, in units of ohm-cm/(elec./cm²). The

TABLE I. Increase $\Delta\rho_i$ of bulk electrical resistivity produced by electron bombardment at an energy of 1.37 Mev.

Run	T (°K) (outlet resistor)	Current (μa/cm²)	Total electron dose (10^{16} elec./cm²)	Resistivity increase $\Delta\rho_i$ (10^{-10} ohm cm)	Resistivity increase per elec./cm² $\Delta\rho_e$ [10^{-27} ohm cm/(elec./cm²)]
1	5	0.52	2.56	2.06	8.05
2	12	0.52	2.20	1.79	8.14
3	13.0	0.52	1.17	0.95	8.12
4	12.0	0.81	1.36	1.10	8.09
5	6 first half 13 second half	0.81	8.39	6.99	8.33
				Weighted average =	8.25

[10] E. H. Sondheimer, in *Advances in Physics* (Taylor and Francis, Ltd., London, 1952), Vol. 1, p. 1.

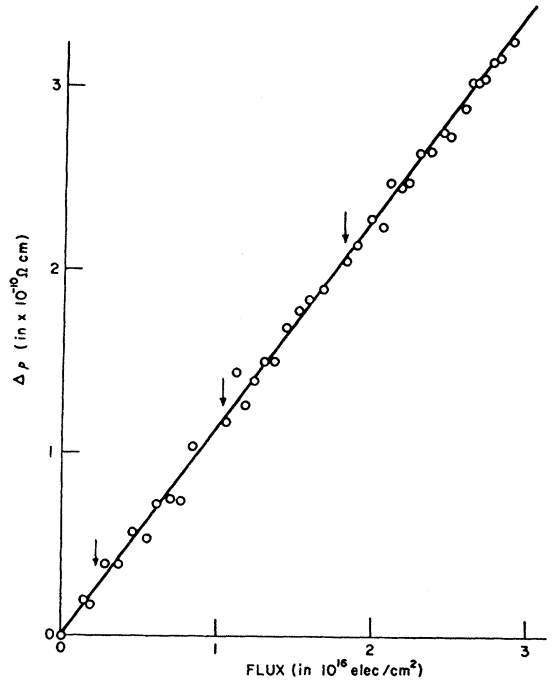

FIG. 5. Beam-on change in resistivity *versus* electron dose. Average beam energy = 1.37 Mev. Although measurements were normally made with the beam off, these measurements were made with the accelerator beam striking the sample. The arrows mark points where the irradiation was interrupted for 15 minutes.

weighted mean of five runs gives $\Delta\rho_e = 8.25 \times 10^{-27}$ ohm cm/(elec./cm²). Variations from run to run represent the errors in resetting the apparatus and are not indicative of the relatively higher precision of separate points in a given run, as can be seen in the results of the longest run to date, which are presented in Table II All resistance measurements leading to the data in Tables I and II were made with the beam off and the sample at 4.2°K.

One run was made during which resistance measurements were made with the beam on, to see if any rapid loss of resistance through annealing was taking place in the short time it took to make the beam-off measurements. The results of this run are presented in Fig. 5. The large scatter of the points here was due to increased circuit noise associated with the beam and accelerator operation. The arrows mark points at which the irradiation was interrupted for 15 minutes, showing that resistivity changes did not occur during these 15-minute annealing periods. Furthermore, the resistivity increments measured with the beam on agree with those obtained with the beam off.

After this initial series of runs at an average energy of 1.37 Mev we undertook to measure $\Delta\rho_e$ at lower bombarding-electron energies. It was necessary to recalibrate the sample current density at each new energy, because of the influence of multiple scattering in the various window foils above the sample.

The electron beam striking the sample is not monoenergetic because the window foils above the sample introduce a considerable amount of energy straggling into the beam. It is difficult, therefore, to specify the precise beam energy at the sample, and both a theoretical and an experimental approach have been used

TABLE II. Bulk resistivity change as a function of electron flux (run 5 of Table I).

Elapsed irradiation time (min)	Resistivity change (10^{-10} ohm cm)	Resistivity change per unit time (10^{-12} ohm cm/min)
71	1.79	2.52
116	2.92	2.52
208.7	5.27	2.53
277.6[a]	6.99	2.52

[a] Integrated flux of 8.39×10^{16} electrons/cm².

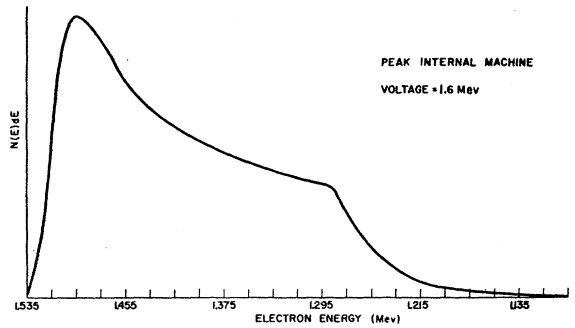

FIG. 6. Calculated distribution of beam electron energies after the beam has passed through the various window foils and penetrated half way into the sample. This distribution was calculated from the Landau theory of energy straggling and from the known energy distribution of the internal accelerator beam.

to solve this beam-energy problem. In the theoretical approach, the theory due to Landau[11] was used to calculate the distribution of electron energies emerging from the foils. Although Hildebrand's[12] high-resolution experiments on the energy distribution of electrons emerging from an aluminum foil bombarded with 624-kev electrons gives somewhat better agreement with the Blunck and Leisegang[13] modification of the Landau theory, the unmodified Landau theory was used for simplicity in calculation. The calculation included, in addition, first-order corrections for the change in energy in passing through the foil system. Increase in effective foil thickness caused by multiple scattering was taken into account by using the procedure of Yang.[14] In order to calculate the Landau distribution it is necessary to know the most probable energy loss. Chen and Warshaw[15] have measured the most probable energy loss for a variety of materials for electron energies overlapping those used in this experiment.

[11] L. Landau, J. Phys. (U.S.S.R.) **8**, 201 (1944).
[12] B. Hildebrand, Phys. Rev. **90**, 378 (1953).
[13] O. Blunck and S. Leisegang, Z. Physik **128**, 500 (1950).
[14] C. N. Yang, Phys. Rev. **84**, 599 (1951).
[15] J. J. L. Chen and S. D. Warshaw, Phys. Rev. **84**, 355 (1951).

Their formula for the most probable energy loss and their values for the average ionization potential are in fair agreement with measurements of Paul and Reich[16] of most probable energy loss for 2.8-Mev and 4.7-Mev electrons, and were employed by us in our calculations.

The final distribution of electron energies also includes the fact that the internal beam itself possesses the distribution of energies characteristic of a chopped sine wave. The results of a typical calculation giving the distribution of electron energies for a peak internal energy in the machine of 1.6 Mev, are shown in Fig. 6. From each such distribution function an average energy $\bar{E}$ was calculated, and the variation of $\bar{E}$ as a function of peak internal energy so calculated is given in Fig. 7. Also included for comparison is the time average of the internal-beam energy distribution minus the average energy loss in traversing the foils calculated from the conventional formula.[17] The method of calculating $\bar{E}$ outlined above weights all electrons equally and does not take into account the fact that high-energy electrons produce more damage than low-energy electrons. The curve of $\Delta\rho_e$ *versus* $\bar{E}$ was used as a weighting

TABLE III. Values of change of resistivity $\Delta\rho_e$ due an irradiation of one elec./cm², at different bombarding energies.

Peak internal machine voltage (in Mev)	Mean energy of the displacement-producing electrons $\bar{E}'$ (in Mev)	Resistivity change $\Delta\rho_e$ [10^{-27} ohm cm/(elec./cm²)]
1.57	1.37	8.25
1.36	1.17	7.17
1.23	1.05	6.40
0.99	0.82	4.37
0.86	0.69	2.74

function which was reapplied to the calculated distribution functions and new values of the average energy $\bar{E}'$ of the damage-producing electrons were calculated. The curve of $\Delta\rho_e$ *versus* $\bar{E}'$ is shifted only slightly from the $\Delta\rho_e$ *versus* $\bar{E}$ curve. The final $\Delta\rho_e$ *versus* $\bar{E}'$ values are given in Table III. The errors include the imprecision in resistivity, beam-current, and peak-voltage measurements.

The experimental approach to the problem of specifying the beam energy at the sample was made by determining the heating effect of the beam for a measured beam current after the beam had passed through the same number of foils that were mounted above the sample. The beam heating experiments were not very precise at low energies but agreed within 10% with the calculated values of $\bar{E}$. In subsequent portions of this paper where certain conclusions are drawn from the curve of $\Delta\rho_e$ *versus* $\bar{E}'$, the values of $\bar{E}$ determined directly by the beam heating measurements were included in evaluating the limits placed on various quantities.

[16] W. Paul and H. Reich, Z. Physik **127**, 429 (1950).
[17] See Seitz and Koehler, reference 1, p. 349.

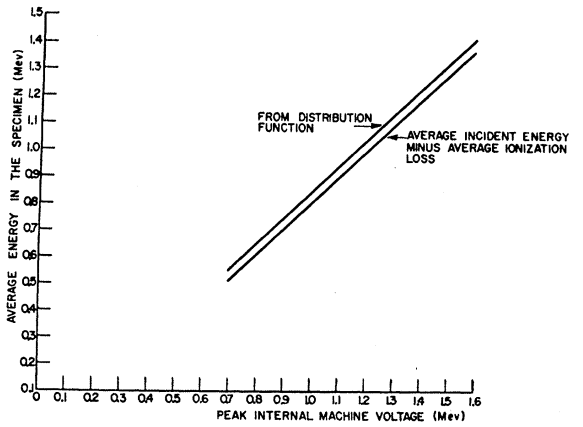

FIG. 7. Calculated average bombarding electron energy in the sample *versus* peak internal machine voltage. The upper curve was obtained by calculating the average energy from several theoretical energy-distribution functions such as shown in Fig. 6. The ordinate for the lower curve is the average energy of the internal accelerator beam minus the average ionization energy loss calculated from the conventional formula.

Annealing experiments were performed using both isochronal and isothermal annealing schedules. The isochronal experiment consisted in pulse-heating the specimen and holding it for ten-minute periods at successively higher temperatures—each ten-minute anneal being followed by a resistivity measurement at 4.2°K. The results of this run are shown in Fig. 8, where the remaining radiation-induced resistivity $\Delta\rho_e$ is plotted as a function of annealing temperature. Essentially no damage anneals out below about 22°K, although about 90% anneals out by 65°K. The peak annealing rate occurs at about 40°K.

The isothermal schedule consisted in pulse heating the specimen to a fixed temperature for a series of arbitrary time intervals, alternated with resistivity measurements at 4.2°K. The results of the isothermal run are shown in Fig. 9. Here four isothermal anneals of a single specimen with a single initial radiation dose were made in sequence at successively higher tempera-

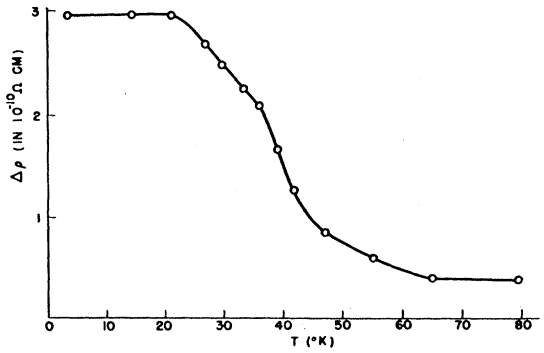

FIG. 8. Isochronal annealing. The experimental points were obtained by pulse heating the specimen and holding it for ten-minute periods at successively higher temperatures—each ten-minute annealing being followed by a resistivity measurement at 4.2°K.

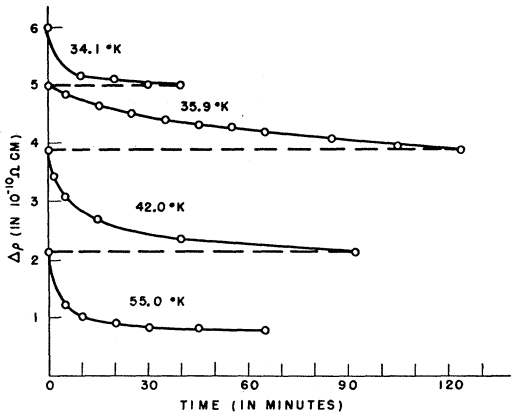

FIG. 9. Isothermal annealing. The experimental points were obtained by pulse heating the specimen to a fixed temperature for a series of arbitrary time intervals, alternated with resistivity measurements at 4.2°K. The four different isothermal curves shown here were made sequentially on a single specimen with a single, initial irradiation.

tures, and hence the shape of each curve except that at 34.1°K depends upon the prior annealing at lower temperatures.

Several of our observations support the view that no significant annealing occurred during irradiation. The data of Table I show that within the experimental uncertainty the same value of resistivity increase per unit electron flux is obtained for quite different sample temperatures and current densities. Table II shows that the resistivity increase is linear in the electron flux, suggesting that neither thermal nor radiation-induced recovery is occurring. The annealing experiments show that no recovery occurs below about 22°K, a temperature that is well above the normal specimen temperature during irradiation. Of course, it is not possible to rule out some extremely rapid annealing process, but the fact that beam-on and beam-off measurements agree, and that Fig. 5 shows that the beam-on measurements before and after a 15-minute beam-off period fall on the same line, show that such annealing would have to occur in a very short time.

DISCUSSION

Damage Production Studies

The differential cross section for electron-nucleus scattering, expressed in terms of the kinetic energy T transferred to the struck nucleus, is given by[18]

$$d\sigma=\pi T_m(1-\beta^2)\left(\frac{Ze^2}{m_e\beta^2c^2}\right)^2 \times\left[1-\beta^2\frac{T}{T_m}+\pi Z\beta\alpha\left\{\left(\frac{T}{T_m}\right)^{\frac{1}{2}}-\frac{T}{T_m}\right\}\right]\frac{dT}{T^2}, \quad (6)$$

[18] See Seitz and Koehler, reference 1. p. 329.

where T_m = maximum kinetic energy that can be transferred to the struck nucleus and is given by

$$T_m=2\frac{m_e}{M}\frac{1}{m_ec^2}(E+2m_ec^2)E, \quad (7)$$

E being the incident electron energy. The other symbols have their conventional meanings.

This expression can be converted to an atomic displacement differential cross section $d\sigma_d$ simply by multiplying it by $P_d(T)$, the probability that the transfer of kinetic energy T to a nucleus will permanently displace it:

$$d\sigma_d=P_d(T)d\sigma. \quad (8)$$

The total cross section for displacement, σ_d, is then obtained by integration of Eq. (8) from $T=0$ to $T=T_m$.

It has been conventionally assumed that the displacement probability is a step function: $P_d(T)=0$ for $T<T_d$, and $P_d(T)=1$ for $T>T_d$. The critical threshold energy T_d for copper has generally been assumed to equal 25 ev as indicated by the approximate calculations of Huntington[19] and by the measurement of the onset of electron-induced damage in copper at liquid nitrogen temperatures by Eggen and Laubenstein.[4] Harrison and Seitz[20] have suggested that better agreement with experiment might be obtained if $P_d(T)$ were assumed to increase more gradually, and Sampson, Hurwitz, and Clancy[21] have considered a linear rise of $P_d(T)$ from zero to unity with increasing T.

Upon calculating the variation of σ_d *versus* bombarding-electron energy [henceforth denoted by $\sigma_d(E)$] for different assumed forms of $P_d(T)$, we found that both the shape and absolute magnitude of $\sigma_d(E)$ are more sensitive to the value of T for which $P_d(T)=\frac{1}{2}$, than to the detailed form of $P_d(T)$, at least for the range of bombarding energies used in this experiment. Our experiments, therefore, give no information about the detailed shape of $P_d(T)$, but do give information about the value of T for which $P_d(T)=\frac{1}{2}$. Since the value of σ_d at each bombarding energy is approximately determined by this quantity, independent of the detailed shape of $P_d(T)$, we have a measure of the absolute value of the displacement cross section.

Figure 10 shows various types of displacement functions used in calculating $\sigma_d(E)$. The $\sigma_d(E)$ curves for different $P_d(T)$ cluster in bands characterized by the value of T for which $P_d(T)=\frac{1}{2}$. An example of this is shown in Fig. 11, which gives curves for different $P_d(T)$ functions which all have $P_d(T)=\frac{1}{2}$ at $T=24$ ev. Calculations for other "average" thresholds than 24 ev show similar behavior. Therefore, in subsequent discussion we shall consider only calculations based on the simple step-function, with the understanding that the threshold energy T_d deduced by comparison of these calculations

[19] H. B. Huntington, Phys. Rev. **93**, 1414 (1954).
[20] W. A. Harrison and F. Seitz, Phys. Rev. **98**, 1530 (1955).
[21] Sampson, Hurwitz, and Clancy, Phys. Rev. **99**, 1657 (1955).

with experiment is to be interpreted as the value of the transferred energy T at which the displacement probability is one-half.

The absolute value of the displacement cross section σ_d is not determined directly from experiment, since the resistivity contribution of a Frenkel pair is not known. However, σ_d is proportional to the measured increase in resistivity per bombarding electron, $\Delta\rho_e$, and hence the shape of the experimental $\Delta\rho_e(E)$ curve is identical with the shape of the $\sigma_d(E)$ curve. The comparison of theory with experiment, therefore, is made with the theoretical and experimental curves all normalized at some value of the energy, which we chose for convenience as $E=1.35$ Mev. Figure 12 shows a normalized plot of calculated $\sigma_d(E)$ curves for various choices of T_d. The narrow cross-hatched region includes the curves of Fig. 11 which were all obtained with different forms of $P_d(T)$ but which had the common feature that $P_d(T)=\frac{1}{2}$ at $T=24$ ev—illustrating again the close clustering of $\sigma_d(E)$ curves for a given $P(T)=\frac{1}{2}$ group.

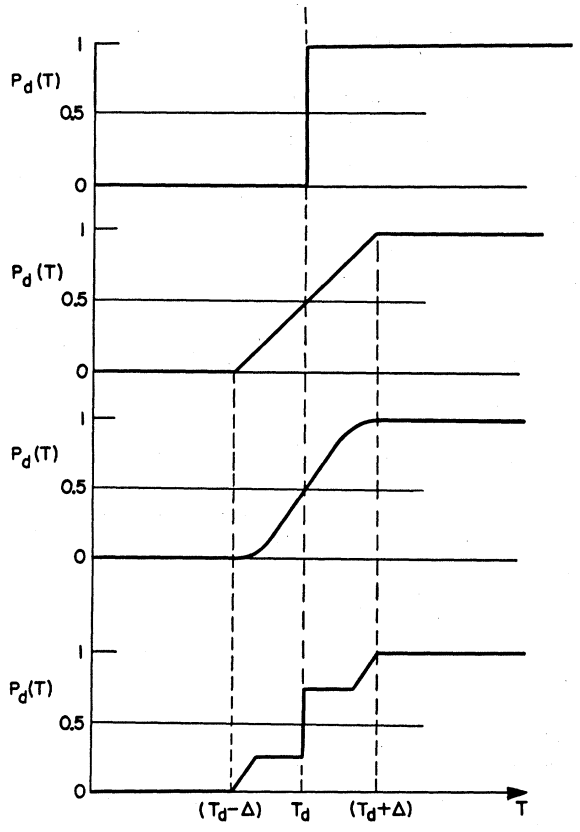

FIG. 10. Different forms for $P_d(T)$, the probability that a struck atom be displaced, as a function of the kinetic energy, T, transferred to the struck atom: (A) step function, (B) linear function, (C) $\sin\chi$ function (where χ goes from $-\pi/2$ at $T-\Delta$ to $+\pi/2$ at $T+\Delta$), and (D) multiple step function. These functions, which are all antisymmetrical about the point $P_d(T)=\frac{1}{2}$, were used to calculate the curves of Fig. 11 which show the variation of displacement cross section with bombarding-electron energy.

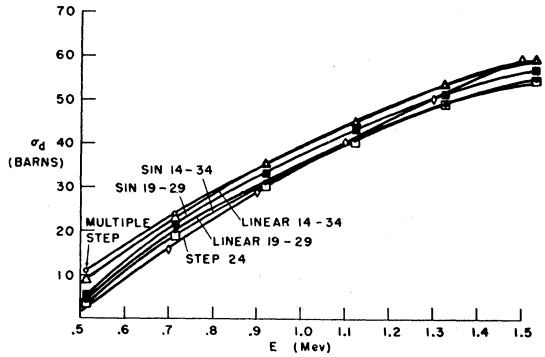

FIG. 11. Displacement cross section, σ_d, *versus* bombarding-electron energy for different forms of the displacement probability, $P_d(T)$, shown in Fig. 10. All these curves have $P_d(T)=\frac{1}{2}$ at a kinetic energy, T, of 24 ev for the struck copper atom. The numbers for each curve give the values of T at which $P_d(T)=0$ and 1.

Figure 13 compares the curves of displacement cross section (calculated using step-function displacement-probability functions) *versus* incident electron-beam energy, with our experimental relative cross section data, the average beam energy associated with each experimental point being calculated from the Landau distribution. From this figure we obtain $T_d=23\pm2$ ev. A value of $T_d=21\pm2$ ev is obtained if the average electron energy determined in the beam-heating experiments is used. The heating experiments give the lower limits on the energy since they are uncorrected for sources of energy loss (e.g., secondary electrons, x-rays, etc.). We shall therefore take $T_d=22\pm3$ ev as our best estimate of T_d. The corresponding value of the displacement cross section at 1.37 Mev is $\sigma_d=(57\pm17)$ barns, determined from a curve like those of Fig. 11, drawn for a step function with $T_d=22$ ev. If one assumes that the damage consists of Frenkel pairs, this value of σ_d together with our previously determined $\Delta\rho_e$ gives a resistivity $\Delta\rho_f=1.45\pm0.5$ μohm cm/atomic % Frenkel pairs.

A similar comparison has been made using theoretical $\sigma_d(E)$ curves calculated by means of the Fuchs analysis[22] which includes the possibility of multiple defect production due to copper atoms that receive sufficient kinetic energy to displace other atoms. This comparison yields $T_d=20\pm4$ ev, $\sigma_d=79\pm26$ barns. However, since the Fuchs analysis probably overestimates the multiplication because the calculation does not include the replacement collision process[23]—the process in which the striking atom in an atom-atom collision may replace the struck atom in the normal lattice site—we have decided to express our results in terms of the production of primary defects.

Implicit in this method of obtaining an absolute cross section by comparison of theoretical and experimental relative cross sections are the assumptions that

[22] R. Fuchs (private communication).
[23] J. Neufeld and W. S. Snyder, Phys. Rev. **99**, 1326 (1955).

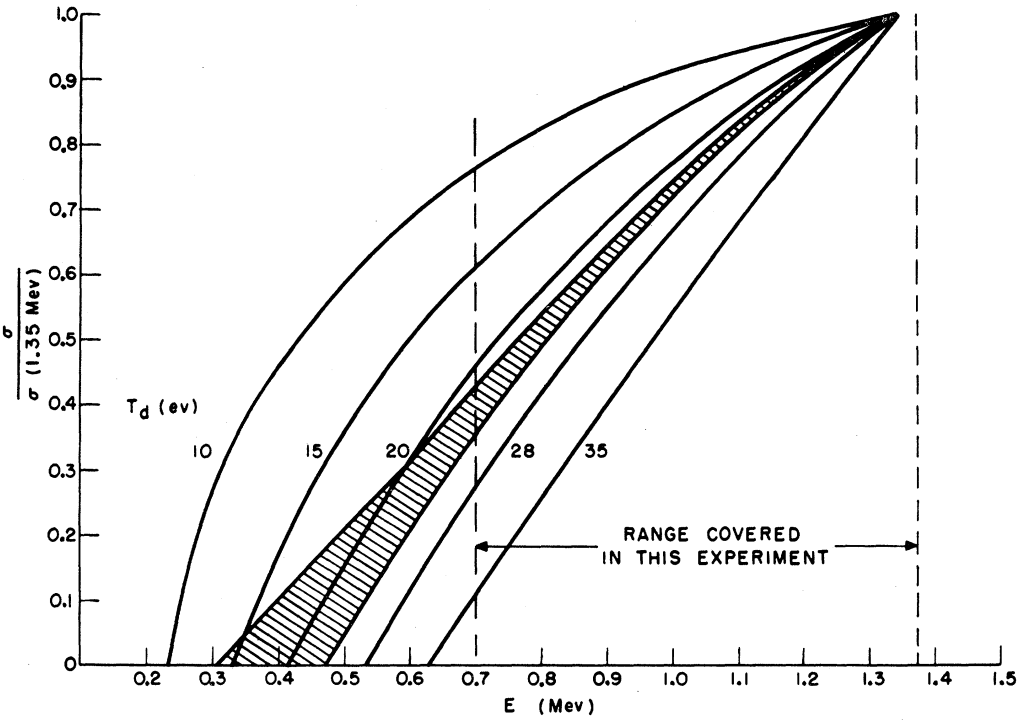

FIG. 12. Displacement cross section normalized at 1.35 Mev, $[\sigma/\sigma(1.35)]$, *versus* bombarding-electron energy. These curves were calculated from Eqs. (6), (7), and (8) of text. The cross-hatched region includes the curves of Fig. 11, all of which had the displacement probability $P_d(T)=\frac{1}{2}$ at 24 ev but with the different forms of $P_d(T)$ shown in Fig. 10. The other curves were calculated under the assumption that $P_d(T)$ is a step function and the numbers refer to the assumed value of the threshold energy.

only one class of defects is produced at different electron energies and that the displacement probability does eventually reach unity. The quoted errors do not include any estimate of the absolute reliability of the cross-section determination, but do include the scatter in fitting the theoretical cross section *versus* energy curves, the absolute errors in determining $\Delta\rho_e$, and the uncertainty due to the difference between the calculated and measured average electron energies.

The final column of Table IV gives some of the various theoretical estimates of $\Delta\rho_f$ and it is seen that the experimental value supports low, rather than high, estimates. The absolute determination outlined above is rather indirect, and experiments are in progress on the change in lattice parameter which should give a more direct and reliable estimate. It is also true that experimental determination of $\Delta\rho_f$ is complicated by the possibility that a significant number of close pairs of interstitials and vacancies are involved in the experiment. Until it is known to what extent the interference between close interstitial and vacancy pairs affects the measured resistivity, and how many such pairs exist, our experimental determination of $\Delta\rho_f$ cannot strictly be compared with the theoretical values in Table IV. However, it would appear unlikely that the true value $\Delta\rho_f$ for separated vacancies and interstitials approaches the large theoretical values.

In both deuteron[2] and neutron[3] irradiations, analyses based on a theoretical value of $\Delta\rho_f=2.7$ μohm cm/atomic % have given defect concentrations a factor of five below that predicted by radiation-damage theory, assuming a 25-ev step-function threshold. Using our values of $T_d=22$ ev and $\Delta\rho_f=1.45$ μohm cm/atomic % in the heavy-particle calculation reduces this discrepancy to a factor of about three. Neufeld and Snyder[23] have included the replacement collision process in the calculation of secondary defect production for heavy-particle damage, and thereby reduce the discrepancy to a factor of $\sim$2.0. It is interesting to inquire whether the remaining discrepancy of 2 to 3 can be accounted for by linear displacement-probability functions that are *consistent with our measured energy dependence*. The calculations of Sampson, Hurwitz, and Clancy[21] indicate that a factor of only about 1.2 is to be obtained in this way, and it seems that the remaining discrepancy will have to be resolved in some other way. The difference probably arises in the considerable complication of the heavy-particle damage process due to the multiplication effect of fast recoil atoms. Qualitatively the relative difference could be explained by the annealing effect of thermal and displacement spikes which are present in the heavy-particle case but absent in the electron bombardment. It may also be that the threshold behavior for atom-atom collisions, which are

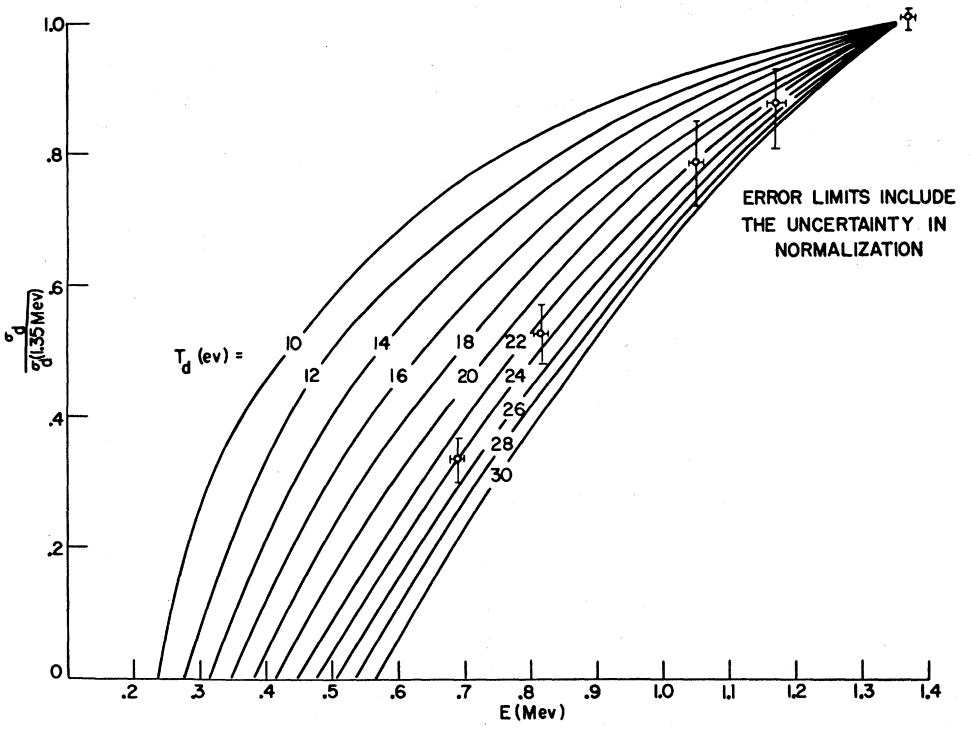

FIG. 13. Comparison of experimental data with theoretical curves of normalized displacement cross section *versus* bombarding electron energy. All the curves were calculated under the assumption that the displacement probability is a step-function and the numbers refer to the assumed value of the threshold energy.

important in the heavy-particle bombardments is somewhat different than the threshold behavior measured here. It clearly would be very interesting to extend damage measurements to high electron energies where the multiplication processes are important, and to bridge the gap between light- and heavy-particle experiments.

Annealing Studies

Annealing experiments of the sort described here potentially provide a great deal of information about the configuration of atoms produced in the initial displacement. For example, if the initial damage process were to correspond to close interstitial-vacancy pairs with an appreciable interaction, such pairs might recombine during annealing according to a first-order rate equation,

$$dn/dt \propto n \exp(-Q/kT), \tag{9}$$

where Q is the energy barrier for recombination. As another example, the interstitials and vacancies may be widely and randomly separated in the damage process. Upon annealing, one class of defects could become mobile and through diffusion find and annihilate the other. The annealing might then proceed according to a second-order rate equation,

$$dn/dt \propto n^2 \exp(-Q/kT), \tag{10}$$

where Q now is the activation energy for diffusion of the mobile defect.

As a third example, the mobile defects might become trapped at randomly distributed trapping centers, leading again to a first-order rate equation if the number of trapping centers is large. In general, the annealing behavior may be complicated by a multiplicity or an admixture of processes of these and other types. Attempts to fit the isothermal annealing data with sums of first- or second-order rate equations show that a minimum of six first-order terms or four second-order terms must be used.

In an attempt to determine an activation energy we have analyzed our isothermal annealing data using Overhauser's slope-matching method[24] for sequential isothermal anneals, and have found that more than a single activation energy is required to describe the data. Overhauser's method does not apply under these conditions. When so many terms must be used and so few experimental points are available, no significance can be attached to the activation energies, beyond noting that they fall in the range of $\sim$0.1 ev.

The isochronal annealing data cannot be described in any simple way either, and it appears that more detailed data are required before the annealing behavior can be interpreted in terms of a detailed model.

Despite the complicated nature of the annealing, it is likely that at least part of the recovery is due to the recombination of interstitials and vacancies, including possible close pairs. The loss of $\sim$90% of the radiation-induced resistivity suggests that most of the defects have participated in whatever processes take place. If we assume that no recombination takes place and that the full resistivity loss results from the motion

[24] A. W. Overhauser, Phys. Rev. **94**, 1551 (1954).

TABLE IV. Theoretical estimates of the resistivity of defects in copper (μohm cm/atomic %).

Reference	Vacancies	Interstitials	Frenkel pairs ($\Delta\rho_f$)
Dexter[a]	0.4	0.6	1.0
Jongenburger[b]	1.3	5.0	6.3
Blatt[c]	0.75–1.0	0.75–1.0	1.5–2.0
Overhauser and Gorman[d]	1.5	10.5	12.0
Harrison[e]	0.8	0.2	1.0
(This paper—experimental value)			1.45±0.5

[a] D. L. Dexter, Phys. Rev. **87**, 768 (1952).
[b] P. Jongenburger, Nature **175**, 545 (1955).
[c] F. J. Blatt, Phys. Rev. **99**, 1708 (1955).
[d] A. W. Overhauser and R. L. Gorman, Phys. Rev. **102**, 676 (1956).
[e] W. Harrison (private communication).

of interstitials to trapping sites, then the resistivity increase left at 80°K is the sum of the resistivity of the initial concentration of vacancies and the resistivity of the trapped interstitials. If the trapped interstitials have zero resistivity, the fact that there has been a net change in resistivity of 10:1 implies that the ratio of interstitial to vacancy resistivities is 9. If the trapped interstitials contribute any resistivity, then the ratio is even higher than 9. From Table IV the maximum theoretical ratio of interstitial resistivity to vacancy resistivity is 7. Further, since our result seems to agree with theories predicting a ratio more like unity, it seems probable that a significant amount of interstitial-vacancy recombination is occurring in our experiment.

The above arguments cannot be pursued persuasively for previous work with neutrons and deuterons which shows a maximum resistivity change of about 50% in this same temperature range. It is not known whether the differences in annealing behavior between the electron and heavy-particle irradiations represent differences in the type of damage produced, or in the specimen purity.

SUMMARY AND CONCLUSIONS

The primary data obtained from our experiments show the following features:

(1) The resistivity increase caused by electron irradiation of copper foils at low temperatures is independent of irradiation rate or time of annealing after irradiation, when the specimen temperature is in the range 4.2°K to about 20°K.

(2) In this temperature range the resistivity increases linearly with the electron dose up to a total of 8.4×10^{16} electrons/cm^2.

(3) 1.37-Mev electrons produce a resistivity increase of $(8.25\pm1.2)\times10^{-27}$ ohm cm/(elec./cm^2).

(4) About ninety percent of the resistivity increase produced by low-temperature irradiation anneals out between 20°K and 65°K, the most rapid annealing occurring near 40°K.

(5) The annealing kinetics are not describable by a simple rate equation with a single activation energy.

From these primary data, with the help of assumptions described in the text, the following additional conclusions can be drawn:

(6) The energy that must be transferred to a copper atom, to give it a displacement probability of $\frac{1}{2}$, is 22 ± 3 ev.

(7) The resistivity of an interstitial-vacancy pair in copper is 1.45 ± 0.5 μohm cm/atomic % of pairs.

This experiment indicates that the simple model which assumes a step-function for the displacement probability, with the threshold energy ~22 ev, gives a fairly good quantitative description of the defect production process. However, it has not been possible to specify the nature of the defects exactly, nor their motion and interaction during an annealing experiment.

ACKNOWLEDGMENTS

We would like to express our gratitude to W. F. Westendorp for aid in the use of the accelerator, to L. B. Nesbitt for technical support in cryogenic matters, to H. B. Huntington for helpful discussions, and to J. C. Fisher for critical review and revision of this manuscript. We are indebted to W. A. Harrison and R. Fuchs for communication of their calculations prior to publication. Thanks are also due J. A. Matuszak for great skill in constructing the cryostat.